Top-down Dendritic Input Increases the Gain of Layer 5 Pyramidal Neurons

Matthew E. Larkum, Walter Senn and Hans-R. Lüscher

Institute of Physiology, University of Bern, Bühlplatz 5, CH-3012 Bern, Switzerland

The cerebral cortex is organized so that an important component of feedback input from higher to lower cortical areas arrives at the distal apical tufts of pyramidal neurons. Yet, distal inputs are predicted to have much less impact on firing than proximal inputs. Here we show that even weak asynchronous dendritic input to the distal tuft region can significantly increase the gain of layer 5 pyramidal neurons and thereby the output of columns in the primary somatosensory cortex of the rat. Noisy currents injected in ramps at different dendritic locations showed that the initial slope of the frequency–current (*f/I*) relationship increases with the distance of the current injection from the soma. The increase was due to the interaction of dendritic depolarization with back-propagating APs which activated dendritic calcium conductances. Gain increases were accompanied by a change of firing mode from isolated spikes to bursting where the timing of bursts coded the presence of coincident somatic and dendritic inputs. We propose that this dendritic gain modulation and the timing of bursts may serve to associate top-down and bottom-up input on different time scales.

Keywords: BAC firing, calcium spike, cortex, dendrite, gain, pyramidal neuron

Introduction

The distal layer 1 fibers coursing across large distances in the cortex carry top-down information from higher cortical areas (Rockland and Pandya, 1979; Felleman and van Essen, 1991; Cauller *et al.*, 1998), feedback information from non-specific thalamocortical pathways (Diamond, 1995) as well as feedback pathways through perirhinal and parahippocampal cortical areas (Lavenex and Amaral, 2000). These inputs make predominantly excitatory (Shao and Burkhalter, 1996) connections to the apical tufts of pyramidal cells (Budd, 1998). Activation of these feedback systems is thought to underlie processes such as attention and binding (Cauller, 1995; Lamme *et al.*, 1998; Olson *et al.*, 2001; Llinás *et al.*, 2002).

Subthreshold distal input to the apical tuft of layer 5 neocortical pyramidal neurons is severely attenuated as it spreads towards the cell body (Berger *et al.*, 2001; Williams and Stuart, 2002) and is shunted by back-propagating action potentials (APs) (Stuart and Häusser, 2001) so that the site of Na^+ AP generation in the axon (Stuart *et al.*, 1997) is hardly effected by it (although see Cauller and Connors, 1994). However, suprathreshold input to the apical tuft generates dendritic APs which lead to multiple APs discharging in a burst-like fashion (Schiller *et al.*, 1997; Larkum and Zhu, 2002). The probability of reaching threshold for this event is facilitated by the interaction between the back-propagating AP and the distal dendritic excitatory postsynaptic potential (EPSP) which relies on a temporal coincidence of 20–30 ms. We refer to this as 'BAC firing' (Larkum *et al.*, 1999). Another coincidence-dependent phenomenon is the boosting of back-propagating APs by dendritic EPSPs (Stuart and Häusser, 2001). Under normal circumstances, pyramidal cells are continuously bombarded by inputs (Steriade *et al.*, 2001) and it is not clear how these timing-dependent mechanisms are influenced by quasi-random fluctuations in membrane potential. Here we investigate this question with noisy, Gaussian-distributed current injections to multiple dendritic sites simultaneously.

Since coincident activation of multiple regions can affect the output of the neuron, it might be expected to modulate the input/output relation (gain) of the neuron. Gain modulation is responsible for a wide range of physiologically relevant behaviors in which different types of information need to be combined (for review see Salinas and Sejnowski, 2001). The underlying computational unit for gain modulation can be realized at the network or single-cell level. It was recently shown on the single-cell level to be dependent on the noise of input conductances (Chance *et al.*, 2002). We show that BAC firing presents another mechanism for gain modulation, which is based on dendritic Ca^{2+} conductances. The activation of distal dendritic Ca^{2+} spikes results in both an increase in gain and the coefficient of variation (CV) of the interspike intervals. In addition, we found that the timing of bursts is correlated with the conjunct input to the distal dendrite and soma within a narrow time window.

The experiments are complemented with a minimal model using two compartments that can fully account for the observed gain modulation and association capabilities of L5 pyramidal neurons. Some of these results have been presented in abstract form (Larkum and Lüscher, 2002).

Materials and Methods

Animal Preparation

Young adult Wistar rats (P26–43, 60–171 g; av. P36, 105 g, n = 32) were anaesthetized with Halothane (Eurim-Pharm, Piding, Germany) and decapitated. Parasagittal slices (300 μm thick) of neocortex were prepared (Sigmann Electronik, Hüffenhardt, Germany). Parasagittal slices were prepared in ice-cold extracellular solution containing (in mM): NaCl 125, KCl 2.5, NaH_2PO_4 1.25, $NaHCO_3$ 25, $MgCl_2$ 1, dextrose 25, $CaCl_2$ 2, at pH 7.4, and transferred to a submersion chamber containing the same solution kept at 37°C for 20–30 min. For recordings, the slices were transferred to a smaller chamber mounted under the microscope and perfused constantly with the oxygenated solution warmed to 34°C. Cadmium (25–100 μM; Fluka, Buchs, Switzerland) was bath applied. Slices were visualized with a 60× objective (Zeiss, Feldbach, Germany) using infrared differential interference contrast optics.

Electrophysiology

L5 pyramidal cells from the somatosensory cortex were chosen if their apical dendrite could be followed far enough to establish that the

dendritic tree was intact. Patch electrodes (5–10 MΩ for soma and 7–15 MΩ for dendrites; borosilicate glass capillaries 2 mm o.d., 1 mm i.d., Hilgenberg, Germany) were made with an electrode puller (Sutter, USA, Model P-97). These were used to make two or three simultaneous whole-cell recordings from different parts of the apical dendrite. One electrode was always placed on the cell soma for recording APs defining the cell's output. Electrodes for recording from the proximal compartment were placed 165–376 μm from the soma and for the distal compartment 445–719 μm from the soma. Pipettes were filled with a solution containing (in mM): potassium gluconate 105, KCl 30, HEPES 10, $MgCl_2$ 2, MgATP 2, Na_2ATP 2, GTP 0.3, at pH 7.3. In addition, all pipettes contained the fluorescent dye Alexa 568 (Molecular Probes, 10 μM) for visualizing the cells during the experiments and biocytin (0.25%) for reconstruction and positive identification of the cell type. Recordings were made with Axoclamp 2B amplifiers (Axon Instruments, Foster City, USA), digitized at 10 kHz with an A/D converter (ITC-18, Instrutech, Port Washington, USA) and acquired on a Macintosh computer using Igor software (Wavemetrics).

Stimulus generation

To generate *in vivo*-like inputs we used the Ornstein–Uhlenbeck method (Tuckwell, 1988) to generate noisy currents with a mean (μ), standard deviation (σ) and correlation length (τ) according to the equation

$$I(t + \mathrm{d}t) = I(t) + \frac{\mu - I(t)}{\tau}\mathrm{d}t + \sigma G_t\sqrt{\frac{2\mathrm{d}t}{\tau}}$$

where $I(t)$ is the injected current and G_t is a random number taken each time step from a Gaussian distribution with mean 0 and standard deviation 1. The correlation length was set to $\tau = 3$ ms, and the time increment, dt, was the same as the sampling interval, 0.1 ms. We chose relatively long (2 s) and small steps (50–100 pA) for the experiments presented here so that the results would be close to steady state. In separate experiments, we examined the effects of injecting shorter steps (data not shown). In these experiments, the gain increased slightly regardless of the site of current injection probably due to the fact that less spike frequency adaptation occurred with shorter steps.

Modelling

The data were reproduced by a two-compartment integrate-and-fire model consisting of a somatic compartment with a transient potassium current to capture the after-hyperpolarization, and a dendritic compartment with a voltage-dependent calcium current (Fig. 7*A*). The two compartments were linked with an ohmic resistance representing the dendritic shaft. An AP was emitted whenever the somatic membrane potential (V_S) exceeded a threshold, which in turn triggered the I_{AHP}. The AP was modelled by clamping V_S for 1 ms to 10 mV and resetting it to the somatic resting potential. Details of the model, equations and the parameters can be found in the Appendix.

Results

Noisy inputs were generated using currents mimicking asynchronous *in vivo* synaptic activity (Steriade *et al.*, 2001). These currents, characterized by their mean (μ), standard deviation (σ) and time correlation length (τ; see Materials and Methods), were injected into the three different somato-dendritic compartments of L5 pyramidal cells (Larkum *et al.*, 2001): the soma, proximal apical dendrite and distal apical dendrite. Note: all experiments shown in this paper used such noisy current injections. We first injected currents into three separate regions alone and determined the *f/I* relations (Fig. 1*A*). These experiments were done as a prelude to examining the more realistic case of input distributed over the dendritic tree (Figures 4 and 5). The firing response of the neuron was measured across the range of possible synaptic input strengths by injecting 'staircase' ramps of increasing μ (Fig. 1*B*; bottom trace), while keeping σ and τ constant at 300 pA and 3 ms, respectively. In 17 experiments at least two simultaneous recordings were made; one from the distal compartment (563 ± 27 μm from the soma) and one from the soma. In 11 of these 17 experiments a third electrode was also placed in the proximal 'coupling region' of the apical dendrite (266 ± 19 μm from the soma). AP firing was assessed from the somatically recorded trace by means of a threshold algorithm.

Threshold and Gain of the f/I Relation Increase with Distance of the Input Location from the Soma

Threshold for noisy current injection causing AP firing at the soma increased with increasing distance of the injection site from the soma (Fig. 1*F*, black dot, somatic current injection; blue dots, proximal dendrite; red dots, distal dendrite). As expected, threshold for noisy current was always lower than for DC current injection at all locations (not shown). Current injection at the soma resulted in APs (Fig. 1*B*) at a similar linear frequency to current (*f/I*) relationship (Fig. 1*C*, black dots) to that already reported for L5 pyramidal neurons (Oakley *et al.*, 2001), and produced attenuated back-propagated APs in the dendrite as shown previously (Stuart *et al.*, 1997).

The gain of the frequency to current relation was assessed by a threshold-linear fit of the non-saturated part of the *f/I* curve, typically up to 80% of the maximal frequency. This gain was determined for each current injection site. For soma and proximal inputs, the mean gain was 0.046 ± 0.001 AP/s/pA ($n = 26$) and 0.056 ± 0.013 AP/s/pA ($n = 11$) respectively (Fig. 1*D*, black and blue dots). For distal current input, the mean gain was significantly higher (0.082 ± 0.0345 AP/s/pA, $n = 17$, Fig. 1*D*, red dot) than for the somatic and proximal compartments. The gain appeared to begin to increase with current injection around 400 μm from the soma and rose as a function of distance from the soma (Fig. 1*E*). The average increase in gain for distal dendritic current injection was 72%, and 22% for proximal current injection. For the rest of the paper we focus on the comparison between the distal compartment and the soma.

Noisy Distal Dendritic Input Results in a Higher CV than Noisy Somatic Input

Once firing threshold was reached with dendritic current injection, mean spike rate rapidly rose to high values (Fig. 1*C*, red line; Fig. 2*B*, triangles). Whereas somatic current injection caused strongly attenuated back-propagating APs (Fig. 2*C*, expanded time scale, black traces), dendritic current injection caused long-lasting depolarizing dendritic events which were often associated with a burst of somatic APs (Fig. 2*D*; arrows and expanded time scale). This burst-firing behavior due to dendritic current injection is also reflected in the high CV of the interspike interval (Fig. 2*B*; inset). When current was injected at the soma, the CV was small and decreased further with increasing current injection. This is consistent with the interpretation that at low currents, the CV is mainly determined by the input current fluctuations (σ), while at high input currents, CV is mainly determined by the mean (μ) of the input current. For distal current injection the situation was quite different. In this condition, the CV was much higher, particularly near threshold where the CV reached values >1. The APs tended to come in bursts, which are mainly determined by the intrinsic properties of the cell rather than the fluctuations in the input current (Williams and Stuart, 1999).

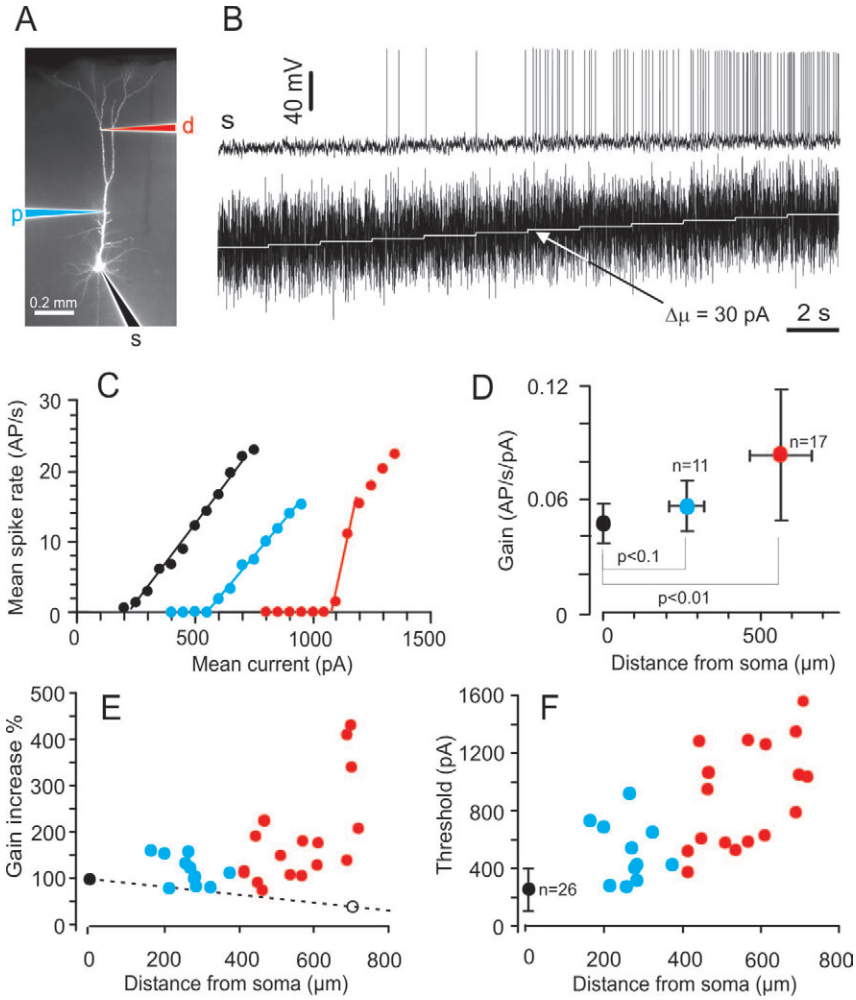

Figure 1. Current to rate transfer functions for noisy input current delivered to different somato-dendritic compartments. (*A*) Fluorescent image of a layer V pyramidal cell together with the three electrodes, one at the soma, one at the proximal dendrite (distance from soma 280 μm) and one at the distal dendrite (distance from soma 690 μm), labelled s (black), p (blue) and d (red), respectively. The three electrodes are in whole-cell configuration and the pipette solution contained 10 μM Alexa 568. (*B*) Upper trace: spike train due to noisy input current in the form of a staircase injected into the soma. Bottom trace; noisy input current injected into the soma (μ_{start} = 0 pA, $\Delta\mu$ = 30 pA, number of steps = 12, step duration = 2.0 s, σ = 300 pA, τ = 3 ms). (*C*) Current to rate transfer functions were obtained by calculating the mean spike rate at the soma for each current step and plotting the rate against the mean current (μ). The black, blue and red transfer function corresponds to current injected into the soma, proximal dendrite or distal dendrite, respectively. The three curves were measured from the same pyramidal cell shown in *A*. They were fitted with a with a threshold linear function (lines) in order to extract their gains (slope) and thresholds. (*D*) Summary for mean gain versus mean distance of the current injection electrode (always measured from the soma; black dot, current injection at the soma; blue dot, current injection at the proximal dendrite; red dot, current injection at the distal dendrite; always ± SD). While the mean gain does not differ for somatic and proximal current injection the mean gain for distal current injection is significantly larger than the gain for the two more proximal locations. The significance levels were always calculated with a paired two-tailed *t*-test. (*E*) Gain increase (% of somatic gain) versus distance of the current injecting electrode from the soma. The dashed line shows the expected decrease of the gain predicted for a passive dendritic tree (the open circle at 700 μm corresponds to an attenuation factor of 0.4; see model in Fig. 7). (*F*) Threshold of the transfer functions versus distance of the current injection electrode.

The gain increase with distal dendritic current injection (Fig. 3*A*; filled circles) disappeared in the presence of the unspecific Ca^{2+} channel blocker Cd^{2+} (Fig. 3*A*; open circles). After application of Cd^{2+}, current threshold was also lowered in some neurons, probably due to an increased cell input resistance. In this cell, the threshold was reduced by 2.5 times after the addition of Cd^{2+}. The expected gain without this increase resistance would therefore be 2.5 times smaller (Fig. 3*A*, dashed line, cf. model in Fig. 7). In addition, blocking calcium channels lowered the CV to levels comparable to somatic current injection (Fig. 3*B*). This decrease of the CV with Cd^{2+} was also reflected in a change from burst firing (Fig. 3*C*,*E*) to regular spiking (Fig. 3*D*). Gain reduction under Cd^{2+} was linearly related to the gain under control conditions (Fig. 3*F*). These results suggest that high gain and large CV for distal current injection is dependent on a dendritic Ca^{2+}-conductance.

Small Somatic Input Increases the Effectiveness of Dendritic Input

Input to the dendrite increased the gain but also had a higher threshold. Under more realistic circumstances, large prolonged input is unlikely to arrive exclusively at the distal tuft. To study the effect of simultaneous input distributed over the dendritic tree we combined current injections into the soma and different dendritic sites. To simplify this part of the study we injected steady-state noisy current at one site while injecting noisy staircase current ramps at the other site. We first looked at the effect of fixed, near threshold somatic input on the gain

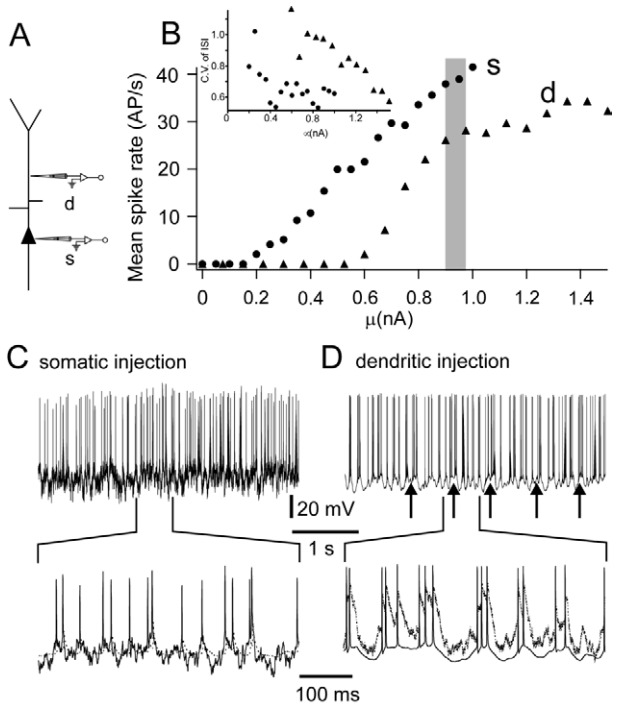

Figure 2. Transfer functions for distal and somatic current injections. (*A*) Schematic drawing of the electrode positions at the soma and distal apical dendrite ($d = 511$ μm from soma). (*B*) Emitted spike rate at the soma as a function of μ (in nA) injected into the soma (filled circles) or into the distal apical dendrite (filled triangles). Parameters of the Gaussian current: $\sigma = 300$ pA, $\tau = 3$ ms, μ was increased stepwise by 100 pA, step duration = 2 s, for 21 steps, starting at $\mu = 0$ nA. Mean spike rate was calculated for each step. The somatic transfer function has a gain of 0.055 AP/s/pA with a threshold current of 150 pA. The transfer function for distal input current has a gain of 0.084 AP/s/pA (a 53% increase) and a threshold at 0.55 nA and. For higher mean currents the spike rate drops back to ~34 AP/s and remains constant thereafter. The grey area indicates the location for which the voltage responses recorded from the soma are shown in *C* and *D*. The inset shows the CV of the mean spike rate for the two transfer functions (using the corresponding symbols). Note that the CV for dendritic input was always higher than for the same somatic input. (*C*) Voltage recordings from the soma for two consecutive current steps of 2 s duration ($\mu = 0.9$ and 0.95 nA) injected into the soma. Below, further expansion of the voltage traces superimposed with the simultaneous recording from the distal apical dendrite (dotted line). (*D*) Same illustration as in *C*, but with the same input current injected into the distal apical dendrite. Somatic current injection leads to single APs, while current injected into the dendrite evokes in addition to single spikes short burst of APs or long, regular spiking during short, plateau-like depolarizations (arrows).

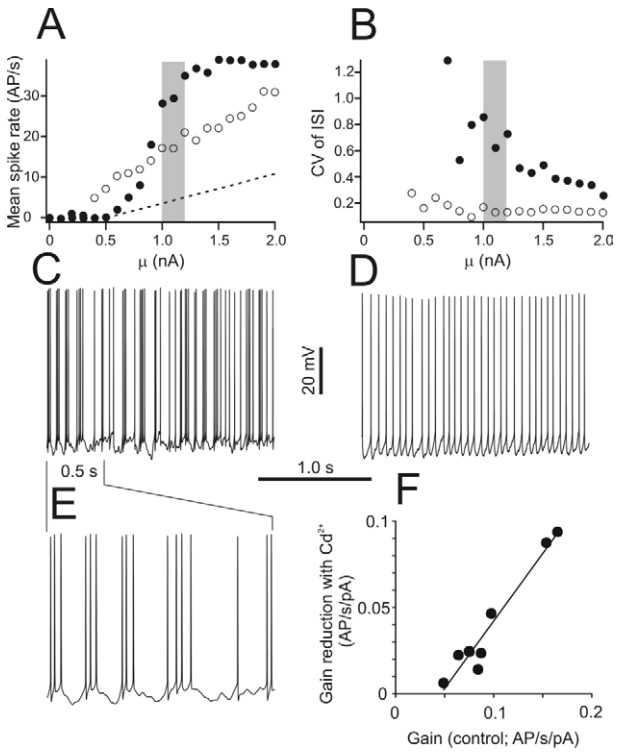

Figure 3. A Ca^{2+}-conductance is responsible for the large gain of the transfer function obtained by distal current injection. (*A*) Transfer function for distal (filled circles, distance: 610 μm from soma) current injection (parameters of the Gaussian current staircase: $\sigma = 300$ pA; $\tau = 3$ ms; 21 steps, step duration = 1 s; $\mu_{start} = 0$ pA, $\Delta\mu =$ 100 pA). Same transfer function after bath application of 100 μM Cd^{2+} (open circles). The shift of the transfer function to the left is due to the increase in the input resistance after the application of Cd^{2+}. The dashed line indicates the predicted *f/I* relation after this effect was compensated (see text). The gain drops from 0.064 to 0.042 AP/s/pA. (*B*) CV of mean spike rate before and after the application of 100 μM Cd^{2+} (same symbols as in *A*). The grey areas in *A* and *B* indicate the two current steps (1.0 and 1.1 nA) for which the expanded somatic voltage recordings are shown in *C* and *D* respectively. (*C*) Somatic voltage recording for two consecutive current steps (1.0 and 1.1 nA) under control condition and (*D*) after bath application of 100 μM Cd^{2+}. Note the irregular firing pattern in *C* compared to the regular firing pattern in *D* which is reflected in the different CV in *B*. (*E*) Expanded time scale of the initial 0.5 s of the somatic voltage recording shown in *C* (note the burst firing with 3–4 APs). (*F*) Gain reduction after bath application of Cd^{2+} (25 to 100 μM) plotted versus control gain.

of distal dendritic input. As shown above, if dendritic input was injected alone (with steps of $\Delta\mu$ = 100 pA from μ = 0 up to 1.1 nA) the AP threshold was reached only with strong current (Fig. 4*A*; last current step with 1.1 nA, red triangles with open arrow). The somatic *f/I* relationship is shown in Fig. 4*A* (black line and filled symbols, labelled s). Injecting 0.25 nA (constant μ) into the soma, which corresponds to a just-subthreshold current for the somatic *f/I* relationship, and combining it with the staircase current injected into the dendrite significantly reduced the threshold for the dendritic *f/I* relationship (red arrow, black and red line, labelled 's+d'). This new *f/I* curve started with a much reduced gain compared to somatic current injection alone since the passive attenuation of dendritic current and was roughly half of the gain obtained when current was injected into the soma alone. With higher dendritic current a second threshold was crossed (around 0.85 nA), and the gain jumped to a value greater than the somatic gain (from 0.85 to 1.1 nA). During this high-gain range in the combined *f/I* curve the CV remained high even at an elevated spike rate (Fig. 4*B*, red symbols). Such an *f/I* curve with two phases was never seen with current injection into the soma alone.

Figure 4*C* shows the spike train resulting from the combined current injection (from which the *f/I* curve in Fig. 4*A*, s+d, was derived). Looking closely at the somatic and dendritic recordings at an expanded time scale reveals that the underlying cause of the high-gain range and the elevated CV was the activation of dendritic regenerative activity. With combined input (Fig. 4*C*), the events triggered by a near threshold current (Fig. 4*D*) were single somatic APs (Fig. 4*D*1) which resulted in small and short back-propagating dendritic APs. Increasing the distal current continued to elicit such single events until the second, high gain-range of the *f/I* relationship was crossed where bursts of 2–4 APs were generated at the soma (Fig. 4*E*, *E*1; black traces). The dendritic potentials that were associated with the bursts (Fig. 4*E*, *E*1; red traces) were much larger in amplitude and broader than with single back-propagating APs.

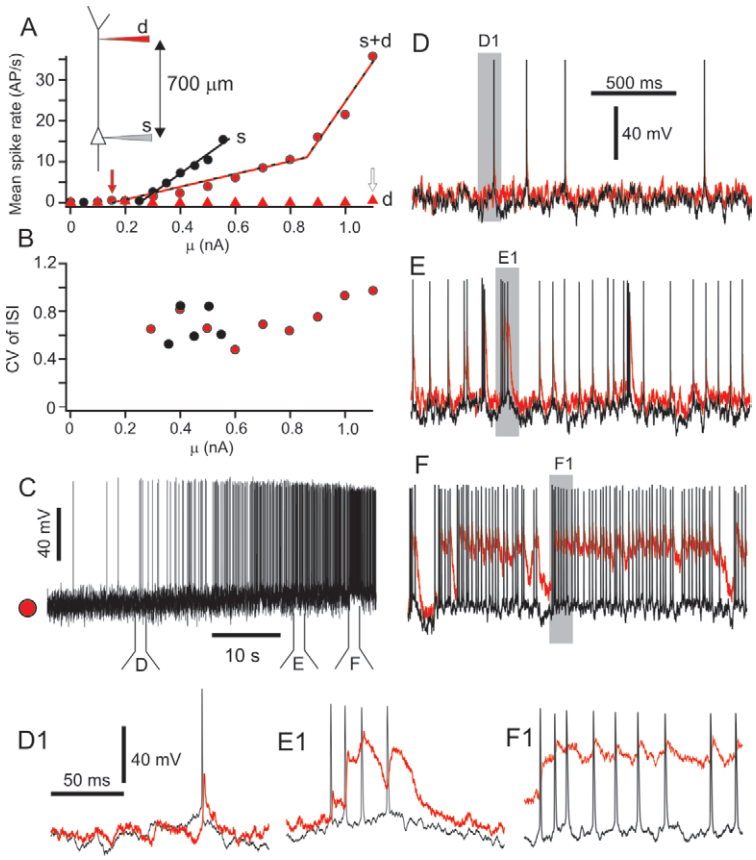

Figure 4. Small somatic background noisy current decreases firing threshold for distal current injection. (*A*) Current to rate transfer functions for somatic (s, black dots) and distal (d, red triangles) current injection in a particular neuron (current parameters for somatic current injection: $\sigma = 300$ pA, $\tau = 3$ ms, $\mu_{start} = 0$ pA, $\Delta\mu = 50$ pA, 12 steps, step duration = 4 s, number of steps = 12) (current parameters for distal current injection: $\sigma = 300$ pA, $\tau = 3$ ms, $\mu_{start} = 0$ pA, $\Delta\mu = 100$ pA, 12 steps, step duration = 4 s, number of steps = 12) Threshold current was 1.05 nA for distal current injection (open arrow). Injection of Gaussian current with a constant mean ($\mu = 0.25$ nA) into the soma and combining it with the staircase current injected into the dendritic location shifts the current to rate transfer function shown with red dots with black lines (s+d) to the left lowering the threshold current from 1.05 nA to approximately 0.15 nA (red arrow). Note the steep increase in the current to rate transfer function at higher mean currents injected into the dendrite. Schema in the inset shows the locations of the two electrodes. (*B*) CV of the mean spike rate for the somatic (black) transfer function and the transfer function for combined (s+d; red) current injection. Note that the CV remains high during the steep rise in the transfer function. (C) Voltage recording from the soma with combined somatic and distal current injection (somatic current injection with constant mean current ($\mu = 250$ pA). This constant current injection at threshold strength renders the distal current very effective in evoking somatic APs. (*D–F*) Corresponding voltage traces at an expanded time scale at the respective times shown in *C*. The superimposed red traces are the voltage recordings from the distally located electrode. A further expansion of the time scale is shown in *D*1, *E*1 and *F*1. Note that at low mean current injected into the dendrite single APs are evoked (*D* and *D*1) whereas with higher mean currents burst of somatic APs are elicited (*E* and *E*1). Further increasing the mean current, long (<500 ms) dendritic plateau potentials are evoked leading to long bursts of high frequency somatic APs.

The change in the gain of the input was therefore most likely due to recruitment of dendritic regenerative activity. At very high dendritic input and simultaneous small somatic input (Fig. 4*F*), long plateau-like potentials were generated in the dendritic compartment which lead to more or less continuous spiking at high rates at the soma.

Dendritic Input Increases Gain of Somatic Input

By reversing the previous experiment (using constant, subthreshold current input to the distal dendritic compartment with staircase input to the somatic compartment) we tested the modulation of the somatic *f/I* relationship by dendritic input (Fig. 5). In this case, constant, small subthreshold input to the dendritic compartment shifted the *f/I* curve (Fig. 5*A*; filled circles) leftwards to much lower current values (Fig. 5*A*; open squares and diamonds). This threshold shift was linearly related to the mean current (µ) injected into the dendritic compartment (Fig. 5*C*). In addition, current injection with constant mean value into the dendritic compartment increased the gain of the somatic *f/I* curve (Fig. 5*A*, *B*). The addition of weak dendritic input combined with somatic input was the most effective regime for causing AP firing. In the example shown in Figure 5, when 250 pA dendritic current was combined with 600 pA somatic current, the firing approximately doubled even though the dendritic input was less than a quarter of the threshold for dendritic current alone (which had a threshold of 1050 pA). This implies that moderate top-down input to the higher layers can significantly increase the output of a cortical column when the layer 5 cells are activated. Note that, in contrast, background activity generating additional somatic input current to layer 5 cells only shifts their *f/I* relationship to the left, but never increases their gain.

Somato-dendritic Coincidence Detection in the Presence of Noisy Input Currents

To examine the mechanism of increased gain with combined currents we determined the typical current trajectory in the soma and the dendrite at the time of an AP and a dendritic

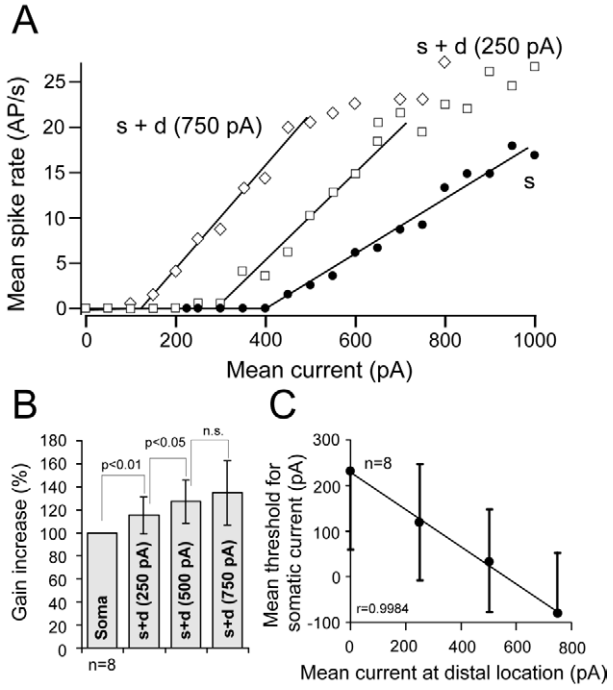

Figure 5. Modulation of the somatic current to rate transfer function by Gaussian current injection with constant mean into distal dendritic location. (*A*) Current to rate transfer function for somatic current injections in a particular neuron (σ = 300 pA, τ = 3 ms, μ_{start} = 0 pA, $\Delta\mu$ = 50 pA, step duration = 2 s, number of steps = 20), together with a noisy current injection into the dendrite with a fixed mean and standard deviation (μ_{Dend} = 0 pA, σ_{Dend} = 0 pA, filled circles; μ_{Dend} = 250 pA, σ_{Dend} = 300 pA, open squares; and μ_{Dend} = 750 pA, σ_{Dend} = 300 pA, open triangles). Note that with increasing mean current applied to the distal apical dendrite the f/I transfer function not only shifts to the left, but also the gain increases. The data points were fitted with a threshold-linear function (lines). (*B*) Summary from eight experiments illustrating the gain increase of the somatic transfer function in combination with distal currents of constant mean. (*C*) Mean threshold for somatic current injection versus constant mean current at distal location.

calcium spike. For this analysis, we extracted the current trajectories generating suprathreshold events in the presence of combined noisy input currents at two sites. The somatic current steps ranged from a mean of 50 pA to 1250 pA, while the simultaneously injected dendritic current ranged from a mean of 250 pA to 750 pA. The noise was throughout 300 pA. We looked for transient dendritic depolarizations above –30 mV which lasted at least 20 ms with simultaneous somatic and dendritic current injection. During the total injection time of 150 s we counted 229 such events and 2272 APs. On average, these transient dendritic depolarizations triggered 2.2 somatic APs within 15 ms (counted from the first spike after dendritic threshold crossing), yielding an estimated intraburst firing rate of 113 Hz. Using the definition of a burst as at least three APs within 20 ms and less than three APs in the preceding 20 ms period, we counted 238 bursts, almost the same number of transient dendritic depolarizations. We conclude that these dendritic depolarizations typically caused the burst firing of a L5 pyramidal cell in response to noisy, distributed inputs.

To determine the typical voltage trajectories that lead to single APs and bursts we calculated spike-triggered and burst-triggered current averages. They were obtained by superimposing the current traces at the time of an arbitrary AP (defined by the threshold crossing of the somatic membrane potential at –15 mV) and at the time of the first AP within a burst (i.e. after threshold crossing of the dendritic membrane potential at –30 mV), respectively (Fig. 6). The spike-triggered average of the somatic current had a much higher peak than the spike-triggered average of the dendritic current (374 pA versus 127 pA; Fig. 6*A*1, *A*2). This indicates that, with injections of noisy currents with similar statistics into soma and dendrite simultaneously, an AP was more likely to be correlated to a current fluctuation at the soma than to a current fluctuation in the dendrite. However, when restricting the analysis to the first spike within a burst, the resulting burst-triggered average current was equally strong or even smaller in the soma than in the dendrite (298 pA versus 358 pA; Fig. 6*B*1,*B*2), contrasting the case of averaging over all spikes (374 and 127 pA; Fig. 6*A*1,*A*2). This shows that bursts were typically associated with both, somatic dendritic input currents, while spikes in general are mainly associated with somatic input. Bursts therefore signaled coincident input into the soma and dendrite. The relationship between bursts and coincident inputs is best demonstrated by the correlation coefficients of combined somatic and dendritic current traces centred at the time of an AP (Fig. 6*A*3), and restricted to the times of the first AP within a burst (Fig. 6*B*3). Coincident somatic and dendritic input current at this time was roughly three times more correlated with a burst than with a single spike (0.55 versus 0.16). Single spikes tended to signal the presence of input to somatic compartment alone, while bursts tended to signal coincident input to both the somatic and dendritic compartment. The coincidence detection window had a width of roughly 30 ms, as found in the case of single pulse injections into soma and dendrite (Larkum *et al.*, 1999). This indicates that even under conditions of random bombardment of inputs, the same mechanisms and dynamics govern firing as with more stereotypical current injections that lead to BAC firing. We therefore refer to bursts generated under these conditions as BAC bursts.

Depending on whether there is coincident dendritic input or not, a back-propagating AP has a very different impact on dendritic membrane potential, and therefore on the cell's firing behavior. A back-propagating AP without concomitant dendritic input decayed with a time constant of roughly 10ms (Fig. 6*A*2). In the presence of simultaneous dendritic input, however, the back-propagating AP tended to trigger strong dendritic depolarization (Fig. 6*B*2). This depolarization, in turn, drove the cell to the high-frequency, irregular firing characteristic of a BAC-burst, indicated by the burst-triggered average of the somatic membrane potential (Fig. 6*B*1).

Minimal Two-compartment Model for BAC Firing

We constructed a two-compartment integrate-and-fire model with a dendritic calcium current (Fig. 7*A*, see Methods and Appendix for details) which reproduced the somatic and dendritic voltage traces, and explains the different properties of the somatic and dendritic *f/I* relationships. The model (Fig. 7*B*, thick red and blue lines) accurately reproduced the *f/I* curves for somatic and dendritic current injections (Fig. 7*B*, red and blue circles), and the somatic and dendritic voltage traces (Fig. 7*C*1,*C*2). With the noise level used in the experiment (σ = 300pA) the individual spike timings were reliably reproduced (66% within ±2 ms in case purely somatic injections, Fig. 7*C*1). When the calcium current in the model was removed, the gain of the *f/I* curve dropped (Fig. 7*B*, right-most thin red line), as observed in the experiment (Fig. 3*A*). In turn,

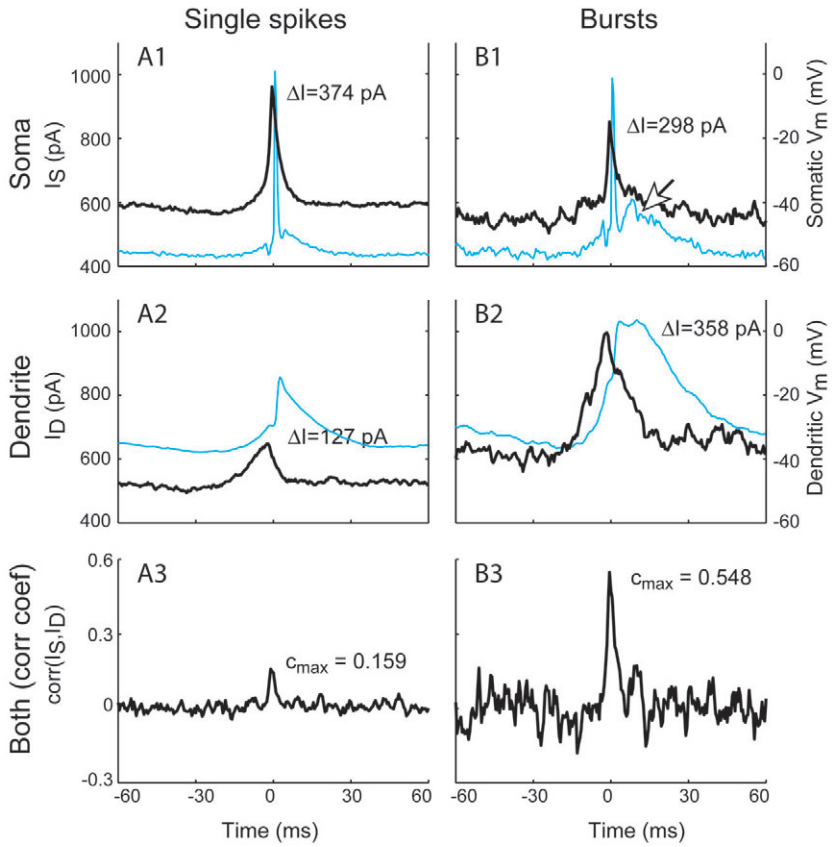

Figure 6. BAC bursts are somato-dendritic coincidence detectors. (*A*) The spike-triggered averages (2272) of the somatic and dendritic current simultaneously injected into one cell. Somatic current contributed almost three times as much to the generation of a spike than the dendritic current (*A*1 versus *A*2, thick black lines, scale left, amplitudes measured from baseline). The spike-triggered average of the somatic and dendritic voltage shows the typical shape of an AP in the soma and back-propagated into the dendrite (*A*1, *A*2, light blue lines, right scale). The somatic and dendritic currents at the times of individual spikes are only weakly correlated (*A*3), indicating that a single spike in general does not require joint somatic and dendritic input. The correlation coefficients are obtained by the point-wise product of the two current traces around the spike times, each subtracted by its mean, $[I_S(t - t_{sp}) - \bar{I}_S]\cdot[I_D(t - t_{sp}) - \bar{I}_D]$, and averaged over all spikes. They are normalized by the square roots of the point-wise autocorrelations of the somatic and dendritic currents. (*B*) Same as in *A*, but averages restricted to the first spike after the onset of the BAC bursts ($n = 229$, see text). The broad averaged somatic voltage trace (*B*1, light blue traces, open arrow) reflects the irregular burst firing induced by a dendritic calcium spike. Note that the average somatic membrane potential during a calcium spike is well above the sodium spike threshold of ~−52 mV (*B*1), while the peak of the dendritic membrane potential is above 0 mV (*B*2). In contrast to the single spike, BAC bursts are likely to be evoked by dendritic input (*B*2) or by a coincident somatic and dendritic input. This is corroborated by the high correlation coefficients of the somatic and dendritic currents, centred at the first spike after the dendritic voltage crossing (*B*3) as opposed to the weak correlation when averaged over all spikes, not restricted to a burst (*A*2). The time window of the somato-dendritic coincidence detection has a width of ~30 ms, as revealed by the burst-triggered average of the dendritic input current (*B*2).

when the calcium currents in the dendritic compartment were activated by concomitant dendritic background input, the gain of the f/I curve increased (Fig. 7*B*, left-most thin blue line). A separation of the two classes of inputs (I_S, I_D) into two compartments is necessary in order to restrict the voltage-dependent interaction of the AP to only one class (I_D).

Threshold-linear Approximation of the f/I Relations

The different f/I relations can be fitted by a threshold-linear transfer function with gain and threshold depending on the amount of noise, the input location, and the calcium dynamics. For somatic DC current of strength μ the threshold-linear f/μ relation takes the form $f = g \cdot (\mu - \theta)$, with gain g_0 and threshold θ. Somatic current fluctuations of amplitude σ decrease the threshold by roughly σ, but also decrease the gain to some value g_s smaller than g (data not shown). The f/μ relation for somatic current injection therefore becomes $f = g_\sigma \cdot (\mu + \sigma - \theta)$. With the parameter values $g_\sigma = 0.05$ AP/s/pA and $\theta = 520$ pA the f/μ relation of the cell shown in Figure 7 is well fitted (middle line). In a passive dendritic tree the means and fluctuations of dendritically injected currents are scaled by an attenuation factor α, and the slope of the f/μ relation for dendritic current is roughly reduced by α, $f = g_{\alpha\sigma} \cdot (\alpha\mu + \alpha\sigma - \theta)$. For the experiment shown in Figure 7 with an electrode placed 700 µm from the soma we have $\alpha \approx 0.4$. The effective gain of the f/μ relation is therefore $\alpha g_{\alpha\sigma} \approx 0.02$ AP/s/pA, while the effective threshold, $(\theta - \alpha\sigma)/\alpha$, roughly increased by $1/\alpha$, see Figure 7*B*, right. Here, the gain reduction due to the attenuation of the mean current (a factor of 0.4) dominated the gain increase due to the reduction of the somatic current fluctuations (a factor of 1.2), so we only consider the former (and therefore identify $g = g_\sigma$). To take into account the dendritic calcium conductances we add a current βf which is proportional to the spike frequency f. The proportionality factor $\beta = \beta(\mu)$ is an increasing function of the dendritic mean current μ which saturates for values above 1000pA. The dendritic f/μ relation in the presence of such regenerative dendritic conductances is implicitely given by $f = g \cdot (\alpha\mu + \alpha\sigma + \beta f - \theta)$, resulting in an increased gain given by $\alpha g/(1 - \beta g)$. With a maximal value $\beta = 15$ pA/AP/s we obtain a gain of 0.08 AP/s/pA (Fig. 7*B*, thin red

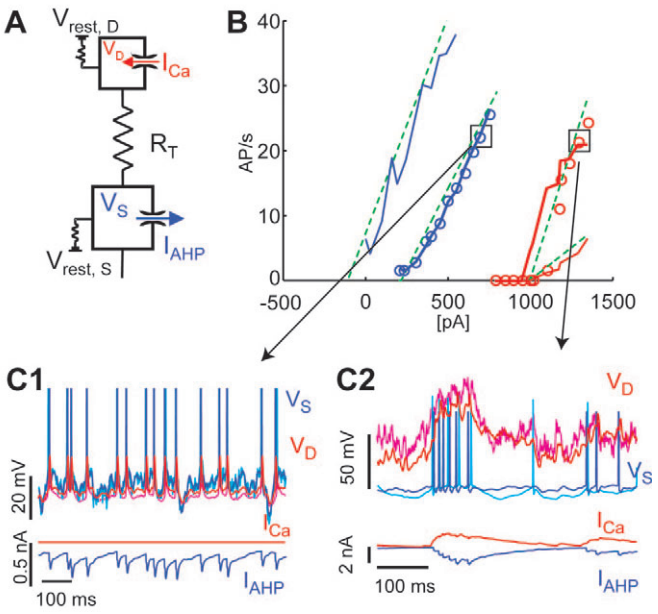

Figure 7. A two-compartment integrate-and-fire model reproduces the somatic and dendritic voltage traces and the *f/I* relationships. (*A*) A voltage-dependent calcium current (I_{Ca}) and a spike-triggered after hyperpolarization current (I_{AHP}) was implemented in the dendritic and somatic compartment, respectively (see lower traces in *C* and Materials and Methods). (*B*) Mean firing rates for somatic and dendritic current injections fit the data well. Circles, experimental data; blue and red lines, model firing rates as a function of the somatic and dendritic current means, respectively; green lines, threshold-linear approximations as described in the text. The restriction of the high gain around 1100 pA is due to the activation window of the dendritic calcium current between −20 and −10 mV. When blocking this current the dendritic *f/I* relationship is determined by the passive attenuation properties (thin red line, right), and therefore has roughly half the gain of the somatic transfer function (thick red line). The thin blue curve to the left represents the mean firing rate of the model neuron as a function of the mean somatic input current in the presence of a noisy dendritic current with $\mu_D = 750$ pA and $\sigma_D = 300$pA. (*C*) Extracts of the somatic and dendritic voltage traces of the model (V_S and V_D, thick blue and red lines, respectively) and the experiment (thin light blue and light red, respectively) when injecting the same current into the model cell and the pyramidal cell. C1) With somatic current injections the membrane potential fluctuations and the spike timings are well reproduced: 66% of the experimental spikes are predicted by the simulation with a precision of ±2 ms. No Ca^{2+}-current is activated in the dendritic compartment (lower red trace). (*C*2) In the case of dendritic current injections the high dendritic membrane potential triggers dendritic calcium spikes (lower red trace) which, in turn, evokes a train of somatic APs (BAC burst).

line), which is higher than the gain of the somatic f/μ relation (Fig. 7*B*, thick red line). When combining somatic and dendritic current inputs, the firing rate is $f = g\,[\mu_S + \alpha\mu_D + \sigma + \beta(\mu_D)f - \theta]$, with $\sigma = \sqrt{\sigma_S^2 + (\alpha\sigma_D)^2}$. Injecting a dendritic current with fixed $\mu_D = 750$ pA (and $\sigma_D = \sigma_S = 300$pA) into the model, we obtain an f/μ_S relation which is fitted with $\beta(\mu_D) = 5$ pA/AP/s. The slope of this frequency to somatic current relationship is $g/[1 - \beta(\mu_D)g] = 0.07$ AP/s/pA (Fig. 7*B*, thin blue line), which is again higher than the slope for somatic current injection alone ($g = 0.05$ AP/s/pA; Fig. 7*B*, thick blue line).

This simple threshold linear approximation of the *f/I* relationship shows how the mean and the noisy component of the somatic and dendritic currents work together in generating the responses. Roughly, the gain for dendritic input is α times smaller and the threshold $1/\alpha$ times larger than for somatic input without dendritic calcium conductances. Only with dendritic calcium events triggered by the back-propagated AP is the gain for dendritic and somato-dendritic inputs elevated above the gain for purely somatic inputs.

Discussion

We have shown the responses of layer 5 pyramidal neurons to noisy current input arriving at three different compartments in various combinations. For each class of inputs we have determined the effectiveness of this input in terms the spike threshold, slope (gain) of the *f/I* relationship and the spike train variability. The results show that distal dendritic input leads to a higher gain and higher variability of the output spike train than somatic and proximal input. Most importantly, even very weak steady-state input to the dendrite increases the gain of proximal inputs implying that top-down input arriving at the distal dendritic tree significantly alters the firing frequency of L5 pyramids that simultaneously receive bottom-up input. While weak somatic input decreases the threshold for distal input, distal input increases the gain and spike train variability for somatic input. Bursts are most likely triggered by joint somatic and dendritic inputs falling within a 30 ms time window. We have shown that even when inputs arrive asynchronously at high rates, BAC firing can still determine the firing properties of layer 5 pyramidal cells. The irregularity of the dendritic input is an important factor because it allows the dendritic calcium conductances to regenerate and sustain their activity over periods of several seconds. In fact, simulating dendritic DC injection in the two-compartment model does not show any gain increase.

Dependence of f/I Relationship on Input Location

One of the new experimental findings of this paper is that the initial slope of the *f/I* curve increases with the distance of the input from the soma. Current injected at the soma showed an approximately linear relationship to firing. A similar relationship was observed with proximal current injection. Distal current injection caused a much steeper rise in the initial part of the *f/I* relationship. Using iontophoretic application of glutamate onto the dendrites Oakley *et al.* (2001) found that firing increase in a step-like manner when threshold was reached, possibly because of the focal nature of the glutamate increase. They conjectured that the jump followed by a plateau is the result of dendritic regenerative activity and not the saturation of glutamate receptors which seems likely in the light of the data we present here. Similarly, the regenerative conductance was found to be Cd^{2+} sensitive (i.e. a voltage-sensitive calcium conductance) in both studies. Persistent Na^+ channels are also known to boost synaptic inputs (Schwindt and Crill, 1995) in proximal regions (Stuart and Sakmann, 1995). Activation of this conductance leads to higher firing rates (Oviedo and Reyes, 2002) which appears to be due to a change in rheobase which shifts the *f/I* relationship to the left without changing the gain (Crill, 1999). In the present study, we saw small increases in firing rates for the proximal region corresponding to Oviedo and Reyes (2002) which could be due to Na^+ conductances, however the greatest increase in firing occurred with more distal current injection and blocking Ca^{2+} channels abolished this increase.

Spike Train Variability

It is well known that the variability (CV) of the interspike interval (ISI) of cortical neurons as observed *in vivo* during behavior is larger than the CV observed *in vitro* by noisy current injection or in simulations with stochastic synaptic inputs (Softky and Koch, 1993; but see Van Vreeskijk and

Sompolinsky, 1996). It has been suggested that the CV of the ISI measured *in vivo* (0.5–1.0) is influenced by network properties. For example, strongly synchronized input (Softky, 1994), or the presence of large but nearly balanced excitatory and inhibitory input which is not present in the slice (Shadlen and Newsome, 1994; Holt *et al.*, 1996). The corollary is that in the slice preparation, without this network activity, the CV of the ISI reflects the CV of the injected input. Indeed, we consistently found that the CV in layer 5 pyramidal neurons was small (typically CV < 0.5) when using noisy current injected at the soma. However, the same noisy current injected at the dendrite consistently elicited spike trains with CV > 0.5. The presence of high CV was dependent on dendritic calcium conductance since it could be reduced to low values comparable to somatic input with the addition of Cd^{2+}. The high CV in our *in vitro* experiments was due to the intrinsic properties of the neuron and not the result of network properties.

Timing of Bursts

The debate about neuronal coding is often reduced to single spike times versus mean frequency (Abeles, 1994). Burst timing offers a third way of encoding both frequency and precision of timing (see also Berger and Lüscher, 2003). The occurrence of a burst within an irregular train of APs tells a postsynaptic neuron that with high probability a strong transient input was jointly present in the dendritic and somatic compartment within a 30 ms time window. If the postsynaptic neuron can detect the presence of bursts (Williams and Stuart, 1999) this information may be propagated throughout the network (Snider *et al.*, 1998). It is interesting to note that both the duration of the burst and the coincidence time window that leads to the burst are approximately of the same duration (~30 ms) which may imply that this level of precision has a special significance in the neocortex. Repetitive somatodendritic associations leading to bursts may also be important for regulating synaptic plasticity (Pike *et al.*, 1999; Golding *et al.*, 2002).

Current Injection versus Dynamic Clamp

To create artificial synaptic input with patch electrodes it is also possible to use the dynamic current clamp technique (Chance *et al.*, 2002). We used the bridge clamp method for this study for technical reasons: for the long recordings made with fine electrodes at multiple dendritic sites, a change in tip resistance has a disproportionate effect on the voltage measured during current injection whereas the magnitude of current injected remains relatively unaffected. Under these conditions, V_m is more robustly determined with bridge clamp and makes comparison between somatic and dendritic current injection possible. Simulations and experiments show that a conductance change in the apical tuft is just as likely to activate calcium regenerativity (Rhodes and Llinás, 2001; Larkum and Zhu, 2002). We confirmed this directly with our two-compartment model (see Appendix) by replacing current injection formulation with simulated synaptic conductances in both compartments. The gain modulation produced by simultaneous synaptic activity at the dendritic and somatic compartments was almost unaffected. This implies that the results shown in this paper would be unchanged by the use of the dynamic clamp method. A similar finding was recently reported by another laboratory (Oviedo and Reyes, 2003). However, if the output frequency is plotted against the frequency of the excitatory input, the gain can be modulated by an additional inhibitory conductance at the dendrite (Prescott and De Koninck, 2003). This mechanism of gain modulation relies on a coordinate transform of the *x*-axis without taking active dendritic conductances into account. Top-down inputs have been shown to be predominantly excitatory (Shao and Burkhalter, 1996) and when activated may lead to a condition in which excitation and inhibition are unbalanced.

Fluctuation-induced Decrease versus Burst-induced Increase of the Gain

Chance *et al.* (2002) showed that an increase in fluctuations of the input leads to a decrease in gain using noisy conductance changes at the somata of L5 pyramidal neurons. When measuring the gain due to noisy current injected into the dendrite (f/I_{dend}), the resulting fluctuations at the soma are smaller than at the site of injection and this decrease would therefore tend to cause an increase in gain. However, the simultaneous attenuation of mean voltage deflection as it propagates to the soma has a larger and opposite affect on the gain. This can be seen by the fact that the gain is larger with somatic current injection in the absence of Ca^{2+} spikes. On the other hand, when measuring the modulation of somatic gain (f/I_{soma}) by steady-state noisy dendritic current, the noise at the dendritic site only serves to increase the total noise at the soma. This increase in noise would decrease the gain as per Chance *et al.* (2002). However, we observed an increase in gain under these conditions, indicating that the mechanisms underlying the dendritic boosting of gain outweigh any fluctuation-based decrease.

Recent simulation studies have implied that asynchronous inputs distributed over the dendritic tree should enhance the overall effectiveness of dendritic input (Rudolph and Destexhe, 2003). Under these conditions the probability of dendritic regenerative events was also increased. In the present study, current was localized to a single dendritic point but was still able to recruit dendritic conductances necessary for enhanced output. Thus, it is possible that under *in vivo* conditions, these mechanisms play an even bigger role in determining output firing.

Point Input versus Distributed Synapses in a Multicompartment Neuron

The effect of inputs distributed over the tuft region should be greatest at the nexus of the various tuft branches which corresponds to the major bifurcation of the apical dendrite (Rhodes and Llinás, 2001). This is also the region with the lowest threshold for Ca^{2+} APs (Larkum and Zhu, 2002). We used a single dendritic electrode to inject current near this region close to the bifurcation which constitutes the best approximation to distributed input over the tuft. This approach does not preclude effects of interactions of inputs on nearby branches (Poirazi *et al.*, 1993; Ariav *et al.*, 2003; Rudolph and Destexhe, 2003) within either the tuft or the basal dendritic compartments but describes the efficacy of the sum of the synaptic currents and active conductances in these compartments in terms of the input/output relation of the neuron (London *et al.*, 2002).

Functional Interpretation

BAC firing is a mechanism for associating joint somatic and dendritic input. Somatic and proximal inputs to layer 5 pyramidal cells typically represent bottom-up input from a specific

sensory modality, while dendritic inputs typically represent top-down information, for instance from other sensory modalities (Cauller, 1995) or from attention steering centres (Shulman *et al.*, 1999; Olson *et al.*, 2001). Our data are compatible with the observation that attention enhances the response of orientation selective cells in a multiplicative way, while the relationship between burst rate and firing rate remains unaffected (McAdams and Maunsell, 1999). It may be advantageous that this kind of global top-down information modulates the output of a cortical column in a different way than the direct, local bottom-up information does (Körding and König, 2000; Rolls, 2000; Siegel *et al.*, 2000). We showed that BAC firing is precisely such a tool which labels the cortical output depending on whether there is simultaneous top-down and bottom-up input or not.

Several modeling studies have pointed out that neurons can have more than one functional compartment that combine to contribute to their firing properties (Rall, 1964; Poirazi *et al.*, 1993; Pinsky and Rinzel, 1994; Mainen and Sejnowski, 1996). BAC firing provides a mechanism for a L5 pyramidal neuron to make 'vertical' associations of cortical inputs that impinge on two different compartments and operate on two time scales. On the slow time scale, associations are manifested in a high gain and variability of the interspike intervals. On the fast time scale, they are manifested in the timing of the calcium spike-mediated bursts in relation to the times of somatic APs (Larkum *et al.*, 1999). These two time scales for vertical associations operate simultaneously. A cell can signal top-down input through a high gain, while at the same time coding specific events through the timing of the bursts. Both time scales are dependent on the association of distal and proximal inputs mediated by the back-propagated AP. Hence, it may be more sensible to view layer 5 pyramidal cells as vertical associators rather than coincidence detectors.

Towards a Canonical Layer 5 Pyramidal Cell

From the results shown in this paper a new picture emerges of how the layer 5 pyramidal cell with its distinct morphological features might operate in an *in vivo* situation (Fig. 8). The back-propagating AP plays a pivotal role in coupling the two-spike initiation zones such that synaptic integration is distributed in time and space. The conspicuously long apical dendrite of the pyramidal neuron and the existence of functionally important inputs at electronically isolated regions has been considered a long-standing enigma (Cauller and Connors, 1994). Indeed, more recently, it has been shown that the existence of I_h in the distal tuft region accentuates the isolation of these inputs (Berger *et al.*, 2001; Williams and Stuart, 2002). However, one advantage of this compartmentalization is that integration can occur simultaneously in two separated regions so that subthreshold inputs to the soma and the tuft essentially do not interact. Once APs are elicited in the initial segment (Fig. 8*A*), the positive feedback mediated by the interaction of these APs with dendritic calcium currents (Fig. 8*B*) completely changes the relative importance of inputs to the cell. Above the 'association threshold', the frequency and timing of the neuronal output is dominated by distal inputs. A simple integrate-and-fire model cannot account for these cellular properties. A model with two compartments, each having its own spike initiation mechanism, is necessary and sufficient to capture this complex phenomenology.

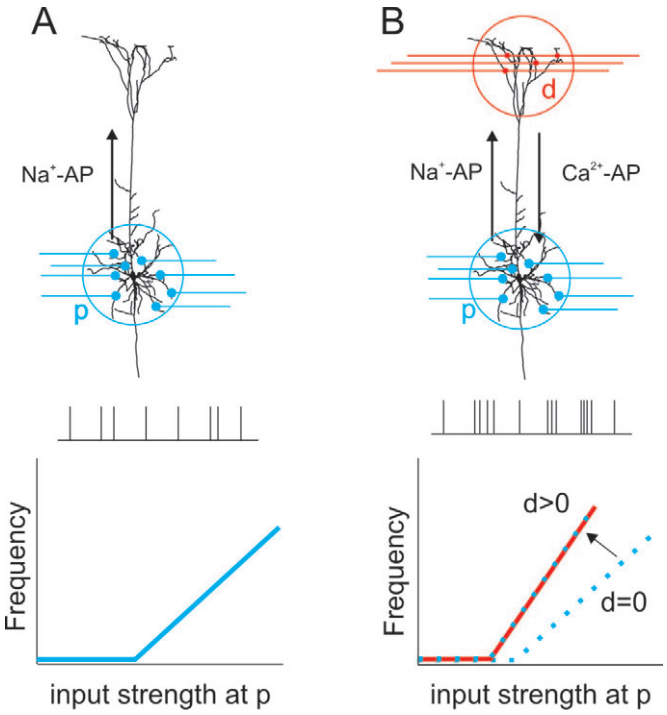

Figure 8. Dendritic gain modulation allows L5 pyramidal cells to associate spatially separated inputs. (*A*) Top panel; L5 pyramidal neuron with synaptic input to basal dendrite and soma only (p), generating the input–output relationship shown in the bottom panel. The firing pattern is nearly regular (spike train, middle). (*B*) Top panel; combination of proximal (p) and weak distal input (d) of constant mean strength shifts the threshold of the input-output relationship to a lower value (bottom panel), and at the same time increases its gain (arrow). This gain increase is the result of the interaction between the back-propagated AP (Na^+-AP) with the weak distal synaptic input, leading to forward propagated Ca^{2+}-AP, which in turn evokes an AP burst at the axonal spike initiation zone. Hence, the association of spatially segregated inputs leads to an increase in the gain and could be signaled to the postsynaptic neuron by the presence of bursts.

Appendix

Details of the Two-compartment Model

The simulation results shown in Figure 7 of the main text were obtained by a two-compartment integrate-and-fire model consisting of a somatic compartment with a transient potassium current and a dendritic compartment with a voltage-dependent calcium current. The two compartments are electrically coupled with a transfer resistance of R_T = 65 MΩ. The compartments have a total membrane resistance of R_S = 50 MΩ and R_D = 43 MΩ, and a total capacitance of C_S = 0.26 nF and C_D = 0.12 nF, respectively. The compartments also have different resting membrane potentials, $V_{rest,S}$ = −70 mV and $V_{rest,D}$ = −60mV, due to action of the hyperpolarization activated unspecific cation current, I_h, located in the dendrite (Berger *et al.*, 2001). The subthreshold dynamics of somatic membrane potential V_S is given by

$$C_S\frac{dV_S}{dt} = \frac{1}{R_S}(V_{rest,S} - V_S) + \frac{1}{R_T}(V_D - V_S) + I_{AHP} + I_{inject,S}$$

and the dynamics of the dendritic membrane potential V_D is given by

$$C_D\frac{dV_D}{dt} = \frac{1}{R_D}(V_{rest,D} - V_D) + \frac{1}{R_T}(V_S - V_D) + I_{Ca} + I_{inject,D}$$

Here, $I_{inject,S/D}$ represents the current injected into the somatic and distal dendritic compartment, respectively.

The potassium current has the form $I_{AHP}(t) = g_{AHP} \cdot (E_K - V_S)\exp(-t/\tau_K)$, with a maximal conductance of g_{AHP} = 4 nS, a reversal potential of E_K = −90 mV, and a decay time constant of τ_K = 80 ms (cf. blue lines in the lowest traces in Fig. 7*C*). The dendritic calcium current has the

form $I_{Ca} = g_{Ca}mh(E_{Ca} - V_D)$, with a maximal conductance g_{Ca} = 70 nS. The activation and inactivation variables, m and h, are characterized by first-order kinetics with time constants τ_m = 15 ms and τ_h = 80 ms, half activations $m_{1/2}$ = –9 mV and $h_{1/2}$ = –21 mV, and slopes s_m = 1/2 mV^{-1} and s_h = –1/2 mV^{-1} of their steady-state functions m_∞ and h_∞, respectively.

Whenever the somatic membrane potential (V_S) exceeds a threshold (θ = –47 mV) an AP is emitted which in turn activates I_{AHP}. The different AP-activated AHP currents are added linearly, as would be expected from a calcium-activated potassium current. The AP is modelled by clamping V_S for 1 ms to 10 mV and resetting it to –52 mV. To mimic the back-propagated AP, the dendritic membrane potential (V_D) is artificially elevated by 10 mV, 3 ms after the crossing somatic threshold. To reproduce the saturation of the *f/I* curves with strong input currents, an additional AP-triggered rectification would be required.

Current Clamp versus Dynamic Clamp

To check whether the dendritic gain modulation is dependent on the use of normal or dynamic current clamp, we repeated the experiments in the two-compartment model using conductances imitating excitatory and inhibitory synaptic inputs. Somatic and dendritic AMPA and $GABA_A$ conductances were mimicked by rectified Ornstein–Uhlenbeck processes with a correlation length of 3 ms. The reversal potentials of the AMPA and GABA receptors were set to 0 and –65 mV, respectively. The mean and variance of the inhibitory somatic and dendritic conductances were fixed to half the mean and variance of the corresponding excitatory conductances. We then increased the mean somatic conductances according to a step protocol with step durations of 2 s and step sizes adjusted to cover the range of mean currents used in the experiment. The variance of the conductances was set such that the variance of the total synaptic currents matched the variance of the injected currents in the original model. We plotted the firing rates against the mean total somatic current generated by the excitatory and inhibitory conductance fluctuations, both with and without dendritic conductance modulation (Fig. A1, dashed lines). These two curves are well approximating the two original *f/I* curves shown in Figure 7*B* left, obtained by simulating direct current injection (with dendritic mean current of 0 and 750 pA, respectively). The relative gain increase due to the additional dendritic drive is similar for normal and dynamic current clamp: with normal current clamp the gain increases by a factor of 1.5 (from 4.5 Hz/100pA to 6.8 Hz/100 pA), and with dynamic clamp it increases by a factor of 1.48 (from 4.8 Hz/100pA to 7.3 Hz/100 pA). We conclude that the dendritic gain modulation is independent of whether the current is directly injected or if a conductance change is simulated with dynamic current clamp.

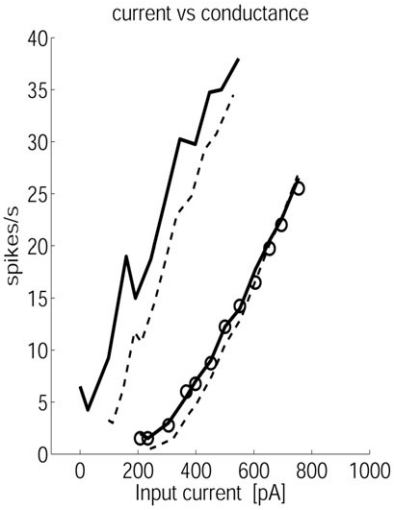

Figure A1. Comparison of the *f/I* curves obtained by simulating current clamp (solid lines, identical two those shown in Fig. 7*B* left) and dynamic clamp (dashed lines). Circles represent data for direct somatic current injection without dendritic modulation. The dashed *f/I* curves show the firing rates against the mean somatic current generated by the somatic excitatory and inhibitory conductances. Without additional dendritic input, the *f/I* curves produced by somatic current and conductance clamp closely matched (two curves on the right). In the presence of dendritic current and dynamic clamp, respectively, the gain of both *f/I* curves increased by a similar factor (of ~1.5). As predicted by the theory, however, the additional leak caused by the dendritic conductance shifts the *f/I* curve to the right.

An intuitive explanation of this is that the relative gain increase remains present because the underlying mechanism, dendritic calcium spikes, is still operating. Dendritic calcium conductances still act multiplicatively because for each somatic AP there is a fixed probability (p) of triggering a calcium spike, which converts the original AP into three APs. This gives a gain increase of $3p$, irrespective of whether the current was generated by synaptic input or by direct injection. Instead of changing the gain, however, an increase in the dendritic conductance leads to a shift of the *f/I* curve to the right as shown by the simulations (Fig. A1) and predicted by the theory (e.g. Holt *et al.*, 1996; Chance *et al.*, 2002).

Because balanced noisy input to the soma lowers the gain of the *f/I* curve (Chance *et al.*, 2002), one may wonder how the additional dendritic noise affects the gain. In fact, the dendritic noise propagates to the soma (with some attenuation factor of roughly 0.4 as shown by Berger *et al.*, 2001) where it decreases the gain of the *f/I* curve. Since in the experiment we not only increased the mean of the dendritic input (from 0 to 750 pA) but also the amplitude of the noise (from 0 to 300 pA, see Fig. 5), the increased noise is effectively counteracting the gain increase produced by the dendritic calcium spikes. If we had only increased the mean of the dendritic input, while leaving the amplitude of the dendritic noise constant (both at 300 pA), the gain of the *f/I* curve would have increased even more. Again, this effect is independent of whether the somatic current was generated by current or dynamic clamp.

Notes

We thank Professor Bert Sakmann, in whose laboratory many of the experiments were performed. We also thank Larry Abbott and Thomas Berger for helpful comments on the manuscript. The research is supported by the SNF grants 31-61335.00 (H.R.L.) and 3152-065234.01 (W.S.), and by the Silva Cases foundation.

The authors declare that they have no competing financial interests.

Address correspondence to Dr Matthew Larkum, Institute of Physiology, University of Bern, Bühlplatz 5, CH-3012 Bern, Switzerland. Email: larkum@pyl.unibe.ch.

References

Abeles M (1994) Firing rates and well-timed events. In: Models of neural networks II (Domany E, Schulten K, van Hemmen JL, eds), ch. 3. New York: Springer-Verlag.

Ariav G, Polsky A, Schiller J (2003) Submillisecond precision of the input/output transformation function mediated by fast sodium dendritic spikes in basal dendrites of CA1 pyramidal neurons. J Neurosci 23:7750–7758.

Berger T, Lüscher H-R (2003) Timing and precision of spike initiation in layer V pyramidal cells of the rat somatosensory cortex. Cereb Cortex 1:274–281.

Berger T, Larkum ME, Lüscher H-R (2001) A high Ih channel density in the distal apical dendrite of layer 5 pyramidal cells increases bidirectional attenuation of EPSPs. J Neurophysiol 85:855–868.

Budd JML (1998) Extrastriate feedback to primary visual cortex in primates: a quantitative analysis of connectivity. Proc R Soc Lond B Biol Sci 265:1037–1044.

Cauller LJ (1995) Layer I of primary sensory neocortex: where top-down converges upon bottom-up. Behav Brain Res 71:163–70.

Cauller LJ, Connors BW (1994) Synaptic physiology of horizontal afferents to layer 1 in slices of rat SI neocortex. J Neurosci 14:751–762.

Cauller LJ, Clancy B, Connors BW (1998) Backward cortical projections to primary somatosensory cortex in rats extend long horizontal axons in layer I. J Comp Neurol 390:297–310.

Chance FS, Abbott LF, Reyes AD (2002) Gain modulation from background synaptic input. Neuron 35:773–782.

Crill WE (1999) Functional implications of dendritic voltage-dependent conductances. J Physiol (Lond) 93:17–21.

Diamond ME (1995) Somatosensory thalamus of the rat. In: Cerebral cortex: the barrel cortex of rodents. Vol. 11, pp. 189–219. New York: Plenum Press.

Felleman DJ, van Essen DC (1991) Distributed hierarchical processing in the primate cerebral cortex. Cereb Cortex 1:1– 47.

Golding NL, Staff NP, Spruston N (2002) Dendritic spikes as a mechanism for cooperative long-term potentiation. Nature 418:326–331.

Holt GR, Softky WR, Koch C, Douglas RJ (1996) Comparison of discharge variability in vitro and in vivo in cat visual cortex neurons. J Neurophysiol 75:1806–1814.

Körding K, König P (2000) Learning with two sites of synaptic integration. Network: Comp Neur Syst 11:1–15.

Lamme VAF, Super H, Spekreijse H (1998) Feedforward, horizontal, and feedback processing in the visual cortex. Curr Opin Neurobiol 8:529–535.

Larkum ME, Lüscher H-R (2002) Cortical gain control mechanism in the distal dendritic compartment of layer V pyramidal neurons. Soc Neurosci Abstr 345.1.

Larkum ME, Zhu JJ (2002) Signaling of layer 1 and whisker-evoked Ca2+ and Na+ APs in distal and terminal dendrites of rat neocortical pyramidal neurons in vitro and in vivo. J Neurosci 22:6991–7005.

Larkum ME, Zhu JJ, Sakmann B (1999) A new cellular mechanism for coupling inputs arriving at different cortical layers. Nature 398:338–341.

Larkum ME, Zhu JJ, Sakmann B (2001) Dendritic mechanisms underlying the coupling of the dendritic with the axonal AP initiation zone of adult layer 5 pyramidal neurons. J Physiol (Lond) 533:447–466.

Lavenex P, Amaral, DG (2000) Hippocampal-neocortical interaction: a hierarchy of associativity. Hippocampus 10:420–430.

Llinás RR, Leznik E, Urbano FJ (2002) Temporal binding via cortical coincidence detection of specific and nonspecific thalamocortical inputs: a voltage-dependent dye-imaging study in mouse brain slices. Proc Natl Acad Sci U S A 99:449–454.

London M, Schreibman A, Hausser M, Larkum ME, Segev I., (2002) The information efficacy of a synapse. Nat Neurosci 5:332–40.

Mainen ZF, Sejnowski TJ (1996) Influence of dendritic structure on firing pattern in model neocortical neurons. Nature 382:363–6.

McAdams CJ, Maunsell HR (1999) Effects of attention on the reliability of individual neurons in monkey visual cortex. Neuron 23:765–773.

Oakley JC, Schwindt PC, Crill WE (2001) Dendritic calcium spikes in layer 5 pyramidal neurons amplify and limit transmission of ligand-gated dendritic current to soma. J Neurophysiol 86:514–527.

Olson IR, Chun MM, Allison T (2001) Contextual guidance of attention. Human intracranial event-related potential evidence for feedback modulation in anatomically early, temporally late stages of visual processing. Brain 124:1417–1425.

Oviedo H, Reyes AD (2002) Boosting of neuronal firing evoked with asynchronous and synchronous inputs to the dendrite. Nat Neurosci 5:261–266.

Oviedo H, Reyes AD (2003) Integrative properties of L5 pyramidal cells. Soc Neurosci Abstr 902.11.

Pike FG, Rhiannon MM, Olding AWA, Paulsen O (1999) Postsynaptic bursting is essential for 'Hebbian' induction of associative long-term potentiation at excitatory synapses in rat hippocampus. J Physiol (Lond) 518:571–576.

Pinsky PF, Rinzel J (1994) Intrinsic and network rhythmogenesis in a reduced Traub model for CA3 neurons. J Comput Neurosci 1:39–60.

Poirazi P, Brannon T, Mel BW (1993) Pyramidal neuron as two-layer neural network. Neuron 27:989–99.

Prescott SA, De Koninck Y (2003) Gain control of firing rate by shunting inhibition: roles of synaptic noise and dendritic saturation. Proc Natl Acad Sci U S A 18:2076–2081.

Rall W (1964) Theoretical significance of dendritic trees for neuronal input–output relations. In: Neural theory and modeling (Reiss RF, ed.). Paolo Alto, CA: Stanford University Press.

Rhodes PA, Llinás RR (2001) Apical tuft input efficacy in layer 5 pyramidal cells from rat visual cortex. J Physiol (Lond) 536:167–187.

Rockland KS, Pandya DN (1979) Laminar origins and terminations of cortical connections of the occipital lobe in the rhesus monkey. Brain Res 179:3–20.

Rolls ET (2000) Hippocampo-cortical and cortico-cortical backprojections. Hippocampus 10:380–388.

Rudolph M, Destexhe A (2003) A fast-conducting, stochastic integrative mode for neocortical neurons in vivo. J Neurosci 23:2466–2476.

Salinas E, Sejnowski TJ (2001) Gain modulation in the central nervous system: where behavior, neurophysiology, and computation meet. Neuroscientist 7:430–440.

Schiller J, Schiller Y, Stuart G, Sakmann B (1997) Calcium action potentials restricted to the distal apical dendrites of rat neocortical pyramidal neurons. J Physiol (Lond) 505:605–616.

Schwindt W, Crill WE (1995) Amplification of synaptic current by persistent sodium conductance in apical dendrite of neocortical neurons. J Neurophysiol 74:2220–2224.

Shadlen MN, Newsome WT (1994) Noise, neural code and cortical organization. Curr Opin Neurobiol 4:569–579.

Shao ZW, Burkhalter A (1996) Different balance of excitation and inhibition in forward and feedback circuits of rat visual cortex. J Neurosci 16:7353–7365.

Shulman GL, Ollinger JM, Akbudak E, Conturo TE, Snyder AZ, Petersen SE, Corbetta M (1999) Areas involved in encoding and applying directional expectations to moving objects. J Neurosci 19:9480–9496.

Siegel M, Körding KP, König P (2000) Integrating top-down and bottom-up sensory processing by somato-dendritic interactions. J Comp Neurosci 8:161–173.

Snider RK, Kabara JF, Roig BR, Bonds AB (1998) Burst firing and modulation of functional connectivity in cat striate cortex. J Neurophysiol 80:730–744.

Softky WR, Koch C (1993) The highly irregular firing of cortical cells is inconsistent with temporal integration of random EPSPs. J Neurosci 13:334–350.

Softky WR (1994) Sub-millisecond coincidence detection in active dendritic trees. Neuroscience 58:13–41.

Steriade M, Timofeev I, Grenier F (2001) Natural waking and sleep states: a view from inside neocortical neurons. J Neurophysiol 85:1969–1985.

Stuart GJ, Sakmann B (1995) Amplification of EPSPs by axosomatic sodium-channels in neocortical pyramidal neurons. Neuron 15:1065–1076.

Stuart GJ, Schiller J, Sakmann B (1997) Action potential initiation and propagation in rat neocortical pyramidal neurons. J Physiol (Lond) 505:617–632.

Stuart GJ, Häusser M (2001) Dendritic coincidence detection of EPSPs and action potentials. Nat Neurosci 4:63–71.

Tuckwell HC (1988) Introduction to theoretical neurobiology. Cambridge: Cambridge University Press.

Van Vreeskijk C, Sompolinsky H (1996) Chaos in neuronal networks with balanced excitatory and inhibitory activity. Science 274:1724–1726.

Williams SR, Stuart GJ (1999) Mechanisms and consequences of action potential burst firing in rat neocortical pyramidal neurons. J Physiol (Lond) 521:467–482.

Williams SR, Stuart GJ (2002) Dependence of EPSP efficacy on synapse location in neocortical pyramidal neurons. Science 295:1907–1910.